Surface Charge and Cellular Processing of Covalently Functionalized Multiwall Carbon Nanotubes Determine Pulmonary Toxicity

Ruibin Li,[†] Xiang Wang,[†] Zhaoxia Ji,[‡] Bingbing Sun,[†] Haiyuan Zhang,[‡] Chong Hyun Chang,[‡] Sijie Lin,[‡] Huan Meng,[†,‡] Yu-Pei Liao,[†] Meiying Wang,[†] Zongxi Li,[§] Angela A. Hwang,[§] Tze-Bin Song,[⊥] Run Xu,[⊥] Yang Yang,[⊥] Jeffrey I. Zink,[§] André E. Nel,[†,‡] and Tian Xia[†,‡,*]

[†]Division of NanoMedicine, Department of Medicine, [‡]California NanoSystems Institute, [§]Department of Chemistry & Biochemisty, and [⊥]Department of Materials Science and Engineering, University of California, Los Angeles, California 90095, United States

ABSTRACT Functionalized carbon nanotubes (*f*-CNTs) are being produced in increased volume because of the ease of dispersion and maintenance of the pristine material physicochemical properties when used in composite materials as well as for other commercial applications. However, the potential adverse effects of *f*-CNTs have not been quantitatively or systematically explored. In this study, we used a library of covalently functionalized multiwall carbon nanotubes (*f*-MWCNTs), established from the same starting material, to assess the impact of surface charge in a predictive toxicological model that relates the tubes' pro-inflammatory and pro-fibrogenic effects at cellular level to the development of pulmonary fibrosis. Carboxylate (COOH), polyethylene glycol (PEG), amine (NH_2), sidewall amine (sw-NH_2), and polyetherimide (PEI)-modified MWCNTs were successfully established from raw or as-prepared (AP-) MWCNTs and comprehensively characterized by TEM, XPS, FTIR, and DLS to obtain information about morphology, length, degree of functionalization, hydrodynamic size, and surface charge. Cellular screening in BEAS-2B and THP-1 cells showed that, compared to AP-MWCNTs, anionic functionalization (COOH and PEG) decreased the production of pro-fibrogenic cytokines and growth factors (including IL-1β, TGF-β1, and PDGF-AA), while neutral and weak cationic functionalization (NH_2 and sw-NH_2) showed intermediary effects. In contrast, the strongly cationic PEI-functionalized tubes induced robust biological effects. These differences could be attributed to differences in cellular uptake and NLRP3 inflammasome activation, which depends on the propensity toward lysosomal damage and cathepsin B release in macrophages. Moreover, the *in vitro* hazard ranking was validated by the pro-fibrogenic potential of the tubes *in vivo*. Compared to pristine MWCNTs, strong cationic PEI-MWCNTs induced significant lung fibrosis, while carboxylation significantly decreased the extent of pulmonary fibrosis. These results demonstrate that surface charge plays an important role in the structure—activity relationships that determine the pro-fibrogenic potential of *f*-CNTs in the lung.

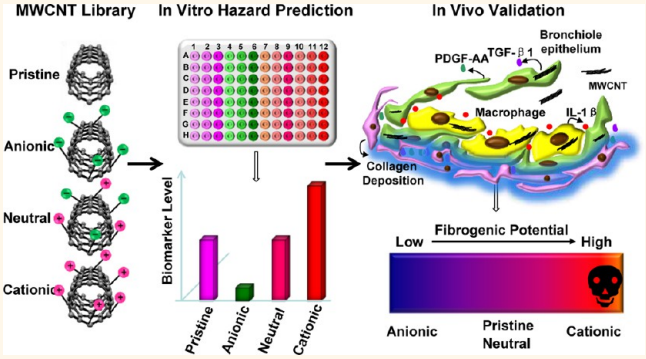

KEYWORDS: multiwall carbon nanotube · surface functionalization · charge · NLRP3 inflammasome · lung fibrosis

Carbon nanotubes (CNTs) are one of the best studied materials in nanoscience and nanotechnology because of their light weight, high conductivity, extraordinary tensile strength, and efficient heat conduction.[1] However, the use of pristine CNTs is limited by low solubility and dispersibility in both organic and inorganic solutions, which makes these materials difficult to handle and process during commercial applications.[2] An effective way of overcoming this difficulty is to functionalize the material surface by introducing hydrophilic chemical groups, which lead to higher dispersibility. Moreover, functionalized CNTs (*f*-CNTs) frequently maintain the unique properties of pristine CNTs, making them easier to process for commercial applications.[3] As a result, *f*-CNTs are widely used as additives,[4] catalysts,[5] sensors,[6] absorbents,[7] intracellular carriers,[8,9] electrodes,[10] and imaging agents.[11] To synthesize *f*-CNTs, covalent and noncovalent approaches can be used, including surface binding of solvophilic molecules or surface coating

* Address correspondence to txia@ucla.edu.

Received for review December 1, 2012 and accepted February 17, 2013.

Published online February 17, 2013
10.1021/nn305567s

with amphiphilic molecules, respectively. Although noncovalent *f*-CNTs are easily prepared, covalent functionalization can be better controlled and tends to be more stable. The two methods most often used for covalent functionalization involve terminal carboxylation and sidewall modification of the tube surface. Carboxyl-modified CNTs (COOH-CNTs) were first reported in 1998,[12] following which a variety of further functionalizations based on the COOH attachment, such as amine (NH_2), polyethylene glycol (PEG), and polyetherimide (PEI) derivatives, were developed for specific use, such as for polyethersulfone membranes,[13] gas sensors,[14] and intracellular carriers.[15−17] Sidewall modification, particularly the attachment of sidewall amines (sw-NH_2), was initially undertaken in the Prato laboratory,[18] where their derivatives were widely used in biology.[19,20]

The rapid growth in *f*-CNT applications has necessitated an understanding of the accompanying adverse health effects, which are being pursued by *in vitro* and *in vivo* toxicological assessment. In general, the *in vitro* studies have shown that *f*-CNTs tend to be safer materials because of improved dispersibility.[21] Pristine CNTs have shown pulmonary toxicity exceeding that of quartz,[22,23] while carboxylated,[24] pluronic-coated,[25] taurine,[26] and polystyrene-functionalized CNTs[27] have been shown to induce less cytokine production, pulmonary inflammation, and fibrosis. In contrast, a recent report showed that NH_2-CNTs lead to increased pulmonary collagen deposition along with increased production of TGF-β1 and IL-6.[28] Although these *in vivo* differences may be attributed to the function of the surface groups, it is known that the complex and multivariate differences in the tube structure derived from different suppliers may also contribute to differences in these response outcomes that are not easy to delineate. Thus, it is imperative to systemically explore the adverse health effects of the functional surface groups on materials prepared from the same batch of pristine CNTs.

In this study, we synthesized a library of well-characterized carboxyl, polyethylene glycol, hexane diamine, sidewall amine, and polyethyleneimine-functionalized multiwall carbon nanotubes (MWCNTs) to systematically study the effect of surface functionalization on tube toxicity in the murine lung. To assess the toxicological impact, we used an established predictive toxicological paradigm to perform mechanistic studies in macrophages and epithelial cells as two key target cell types that play a role in the pathophysiology of pulmonary fibrosis.[25] The cooperation between these cells determines IL-1β, TGF-β, and PDGF production, which is responsible for epithelial−mesenchymal transition (EMT), chronic inflammation, and fibrosis in the lung.[25] These mechanism-based cellular studies allow *in vitro* hazard ranking that can be compared to related biomarker responses and collagen deposition in the animal lungs.[24,25] Our results show that, compared to pristine MWCNTs, anionic functionalization significantly decreases cellular and lung pro-fibrogenic effects, while the attachment of cationic PEI leads to a significant increase in fibrosis. Neutral and weak cationic *f*-MWCNTs have intermediary effects. This study demonstrates the utility of a predictive toxicological approach, allowing us to forecast the injurious effects of the functionalized CNTs based on their structure−activity relationships *in vitro*. This information is important for the regulatory consideration as well as informative for the safer design of MWCNTs for biomedical use.

RESULTS

Covalent Synthesis and Characterization of *f*-MWCNTs. To systemically study pulmonary injury by functionalized tubes, we established a library of covalent *f*-MWCNTs that are frequently used for commercial applications. In order to avoid carrying out the analysis with tubes from different sources, we used pristine or "as-prepared" (AP) MWCNTs from Cheap Tubes to prepare carboxyl (COOH) and sidewall amine (sw-NH_2)-functionalized MWCNTs as a first step. In addition, we also prepared carboxyl-converted PEI-MWCNTs (cc-PEI-MWCNTs) to study the strong cationic effects of the branched amino groups as well as their conversion to a COOH group after reaction with succinic anhydride.[29] As shown in Figure 1, the COOH-MWCNTs were synthesized *via* oxidization and then acylated to prepare polyethylene glycol (PEG), hexane diamine (NH_2), and polyethyleneimine (PEI) *f*-MWCNTs. The PEG modification was introduced by esterification of the acylated COOH-MWCNTs with polyethylene glycol, while NH_2 and PEI-MWCNTs were synthesized by ammonolysis of the acylated tubes with hexane diamine and polyethyleneimine, respectively.[30] The sw-NH_2-MWCNTs were synthesized *via* 1,3-dipolar cyclization reaction to produce a relatively weak cationic tube.

This *f*-MWCNT library was comprehensively characterized for the placement and quantity of functionalized surface groups by Fourier transform infrared spectroscopy (FTIR) and X-ray photoelectron spectroscopy (XPS). Shape and size were assessed by transmission electron microscopy (TEM), hydrodynamic diameter by dynamic light scattering (DLS), and surface charge by zeta-potential analysis. Figure 2A shows TEM images of the tubes, which demonstrate typical 1-D fiber-like structures of different length. Because oxidative functionalization splices and converts pristine to shorter carboxylic tubes, COOH-MWCNTs as well as their PEG, NH_2, PEI, and cc-PEI-functionalized derivatives display shorter lengths of ∼200−450 nm compared to the 570−580 nm length of AP- and sw-NH_2 tubes (Supporting Information Figure S1). The hydrodynamic diameter and zeta-potential of tubes dispersed in water are shown in Table 1. The hydrodynamic size of COOH, PEG, PEI-MWCNTs, as well as cc-PEI-MWCNTs in water is 140−290 nm, which is much smaller than AP, NH_2, and sw-NH_2-MWCNTs with 1900−2300 nm hydrodynamic size. This is not surprising

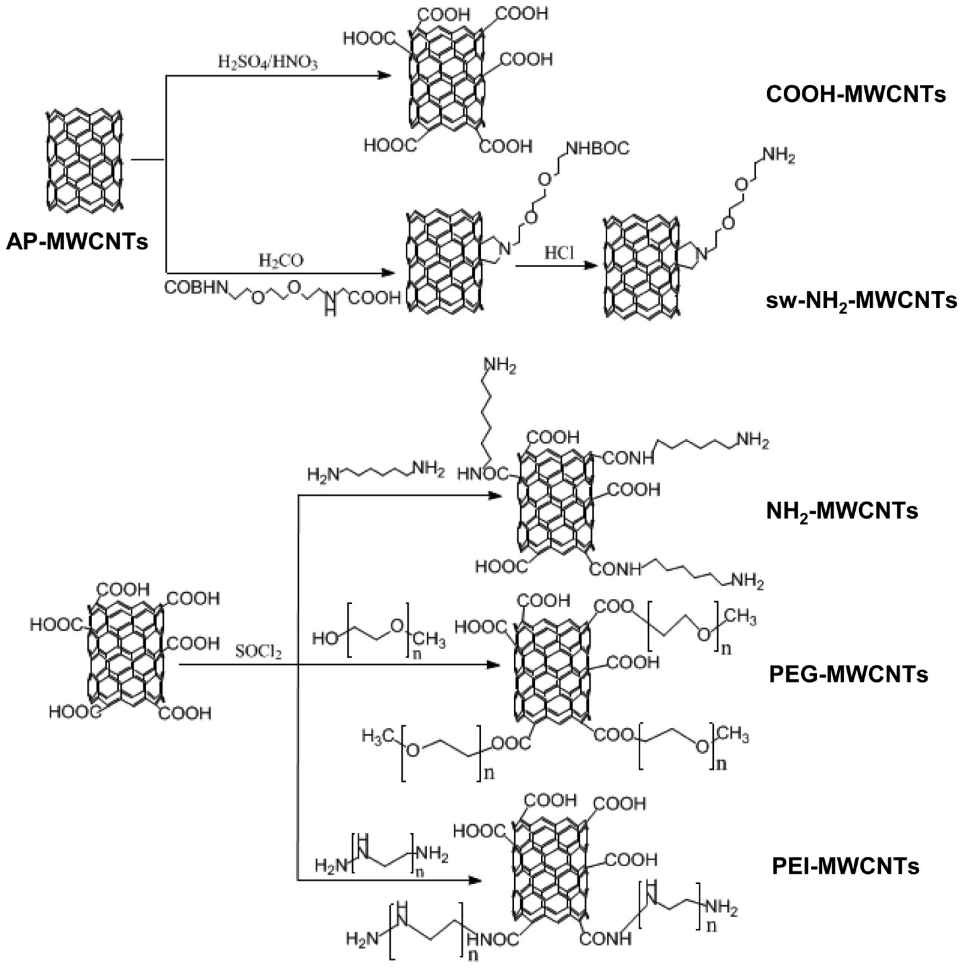

Figure 1. Synthesis scheme for *f*-MWCNTs. AP-MWCNTs were purchased from Cheap Tubes Inc. COOH-MWCNTs were prepared *via* an oxidization reaction of MWCNTs in H_2SO_4/HNO_3. Synthesis of sw-NH_2-MWCNTs included 1,3-dipolar cyclization reaction and a subsequent acid treatment to remove the Boc group. To prepare other functionalized tubes, COOH-MWCNTs were further activated in $SOCl_2$ to produce acylated tubes. PEG, NH_2, and PEI-MWCNTs were derived by binding PEG, hexane diamine, or PEI on acylated COOH-MWCNTs.

because the zeta-potential values of COOH, PEG, PEI, and cc-PEI-MWCNTs were −52.61, −45.46, +53.33, and −23.21 mV, respectively, which could provide strong electrostatic repulsion in aqueous solution. In contrast, the large hydrodynamic size of NH_2 and sw-NH_2-MWCNTs may be due to the low zeta-potential (−2.35 and 12.95 mV), and lack of electrostatic repulsion as a result of the comparatively low degree of functionalization. After dispersion into BEGM supplemented with BSA plus dipalmitoylphosphatidylcholine (DPPC), RPMI 1640 supplemented with 10% FBS (c-RPMI 1640) or PBS supplemented with BSA plus DPPC, as shown in Table S1, the hydrodynamic diameter of AP, COOH, PEG, NH_2, and sw-NH_2-MWCNTs assumes diameters of 200−400 nm while PEI-MWCNTs form aggregates of 1500−2500 nm. The formation of large PEI-MWCNT aggregates is the result of the disappearance of the surface of the double layer as a result of the interaction of anions and proteins with the positive tube surface.[31,32] All of these tubes show approximately similar zeta-potential, in the range from −3 to −10 mV due to the neutralization of surface charge by anion electrolytes or proteins.[33]

To confirm successful covalent modification, solid-state FTIR was performed to show the presence of the peaks that characterize each of these functional groups on the tube surface (Figure 2B). The presence of carboxylic groups was confirmed by C═O stretching vibrations at 1730 cm^{-1} as well as O−H stretching vibrations at 3430 cm^{-1}. These carboxylic group bands were also present in the incomplete functionalized PEG, NH_2, and PEI-MWCNTs. PEG and sw-NH_2-MWCNTs displayed C−O stretching vibrations that originate from the ester groups at 1105 cm^{-1}. NH_2-MWCNTs, sw-NH_2-MWCNTs, as well as PEI-MWCNTs had common peaks at 1635 and 1206 cm^{-1}, which can be assigned to the N−H deformation vibration of primary amine groups as well as the C−N stretching vibrations, respectively.[30] The FTIR of cc-PEI-MWCNTs shows an O−H stretching vibration peak at 3430 cm^{-1} and a C═O peak at 1730 cm^{-1} demonstrating the COOH group, while the N−H peak and C−N peaks demonstrate the presence of residual amino groups (Figure S1).

In order to quantify the extent of functionalization, which determines the charge and suspension stability

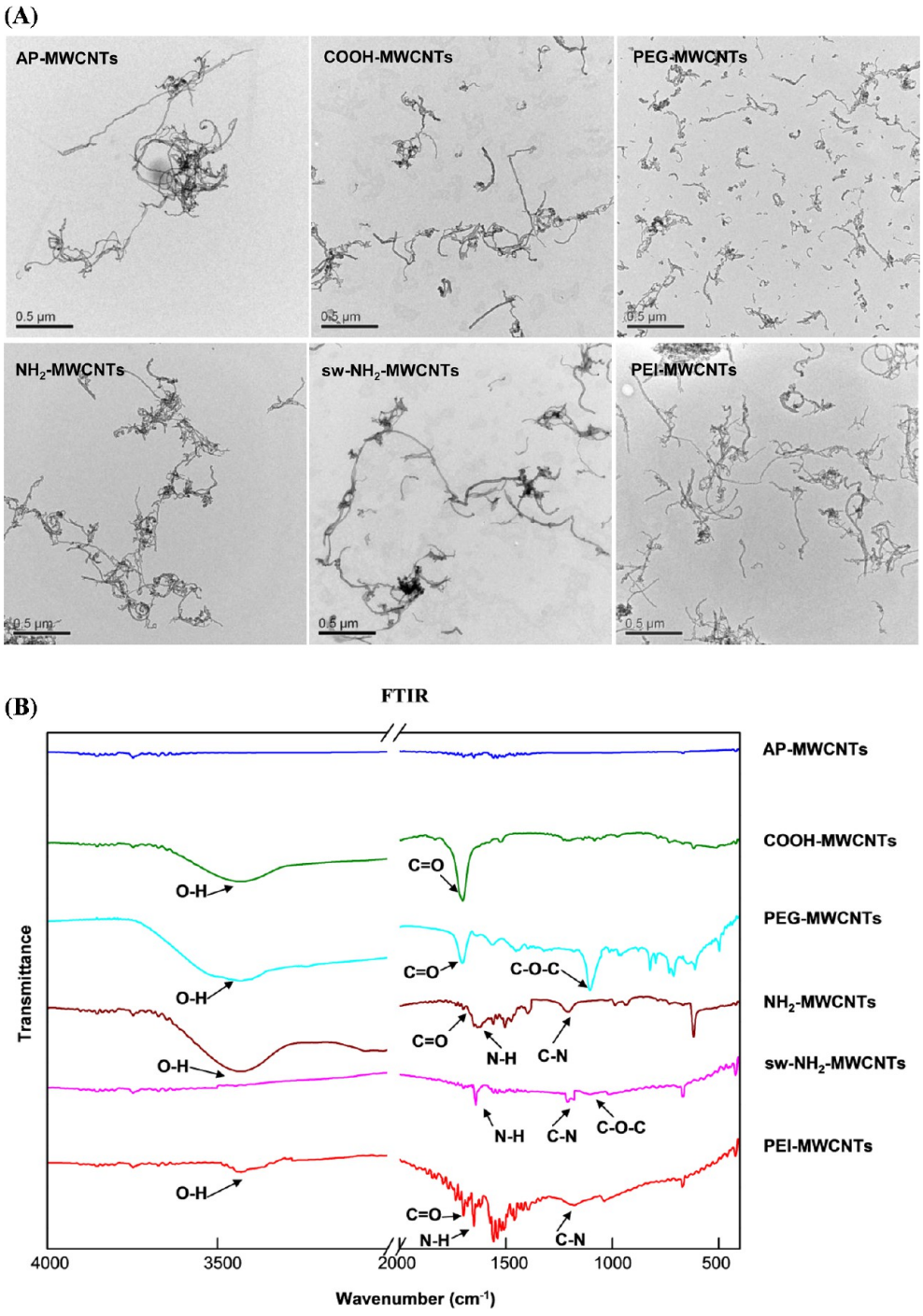

Figure 2. Physicochemical characterization of *f*-MWCNTs. (A) TEM images show the length, diameter, and structure of MWCNTs. (B) FTIR spectra of *f*-MWCNTs show the presence of different functional groups and confirm successful covalent surface modification of the MWCNTs.

of the hydrophobic surface on the raw tubes, we used X-ray photoelectron spectroscopic analysis (XPS). The elemental composition analysis in Table S2 shows the atomic percentage (atom %) nitrogen and/or oxygen in the *f*-MWCNTs. The C1s core level peak positions of the carbon atoms are close to 284.6 eV, while the peak positions for nitrogen and oxygen were centered at ~400.2 and 532.5 eV, respectively. AP-MWCNTs showed a low level (~0.5%) of oxygen, which is typical for pristine MWCNTs.[34] After carboxylation, the oxygen percentage on the COOH-MWCNT tube surface increased to 9.24%, which agrees with the percentages of PEG (8.94%), NH_2 (9.96%), and PEI-MWCNTs (8.42%). In accordance with their direct synthesis from pristine tubes, sw-NH_2-MWCNTs showed low percentages of oxygen (1.42%) and nitrogen (0.6%) on the surfaces. NH_2-MWCNTs showed nitrogen content of 1.46%, while the corresponding value for PEI-MWCNTs was 5.66%.

TABLE 1. Hydrodynamic Diameter and Zeta-Potential of *f*-MWCNTs in Water

MWCNTs	hydrodynamic diameter (nm)	zeta-potential (mV)
AP	2302 ± 56	−10.52 ± 2.73
COOH	141 ± 0	−52.61 ± 1.22
PEG	148 ± 1	−45.46 ± 1.05
NH_2	1953 ± 233	−2.35 ± 3.28
sw-NH_2	2279 ± 257	12.95 ± 2.94
PEI	251 ± 4	53.33 ± 1.82
cc-PEI	287 ± 7	−23.21 ± 1.56

Suspension stability index in cell culture media, as a reflection of the sedimentation rate of the tubes, determines their bioavailability under tissue culture conditions.[35] As shown in Figure S2, the anionic COOH and PEG-MWCNTs displayed the highest stability with *ca.* 95% remaining after 20 h, followed by AP, NH_2, and sw-NH_2-MWCNTs, which exhibited more or less the same level of stability around 70%. Instead, cationic PEI-MWCNTs were the least stable with only ~20% of tubes remaining in suspension by 20 h. All considered, these results suggest that the more rapid sedimentation rate of PEI-MWCNTs would make them more bioavailable to cells settling at the bottom of the wells. However, under *in vivo* conditions, sedimentation may play a lesser role in tube-induced effects because of the relatively thin layer of lung lining fluid.

Pro-fibrogenic Cellular Responses Are Dependent on *f*-MWCNT Charge. These experiments were carried out in the myeloid cell line, THP-1, a macrophage-like cell line, as well as BEAS-2B cells, an immortalized human bronchial epithelial cell line. We have successfully used these cells to assess pro-fibrogenic cytokine and growth factor production of aggregated and dispersed AP-MWCNTs, showing that the response differences between those tubes at the cellular level accurately reflect their propensity to induce pro-fibrogenic responses in the lung.[24,25] First, we determined the cytotoxicity of *f*-MWCNTs by conducting a MTS assay 24 h after their introduction to the cultures.[36,37] This demonstrated a lack of cellular toxicity at tube concentrations as high as 120 μg/mL (Figure S3). THP-1 cells were used to measure IL-1β production, which represents a major cytokine used by pulmonary macrophages to initiate a cascade of events in cooperation with epithelial cells that culminate in pulmonary fibrosis.[38] We also used coculture of THP-1 with BEAS-2B cells to assess TGF-β1 and PDGF-AA production as relevant pro-fibrogenic growth factors, which in concert with IL-1β determines fibroblast proliferation and collagen deposition in the lung.[39] Following incubation with 60 μg/mL *f*-MWCNTs for 24 h, IL-1β and growth factor production in the cellular supernatants were examined by ELISA (Figure 3A). AP-MWCNTs served as a positive control.[40] All MWCNTs, except for the COOH tubes, induced significant increased levels of IL-1β, TGF-β1, and PDGF-AA compared to untreated cells. However, anionic COOH and PEG-MWCNTs showed significant lower production of all three factors compared to AP-MWCNTs. Instead, NH_2-MWCNTs exhibited a slight but significant decrease of IL-1β and PDGF-AA production compared to the pristine tubes, while sw-NH_2-MWCNTs displayed similar levels of IL-1β and PDGF-AA production. However, sw-NH_2-MWCNTs induced a significant increase in TGF-β1 production, while PEI-MWCNTs induced significantly higher responses of the pro-fibrogenic factors compared to all of the other tubes. As demonstrated in Figure S4A, the cytokine production induced by different MWCNTs was dose-dependent.

Except for surface charge, the length of the CNTs may influence their pro-fibrogenic potential. For this reason, we measured tube length by TEM, as shown in Table S3. While PEG, COOH, NH_2, and PEI-functionalized tubes show a slight decrease in length, sw-NH_2-MWCNTs showed a length similar to AP-MWCNTs. Thus, as a result of the minor effect on tube length, there was no noticeable correlation between this physicochemical parameter and pulmonary injury in our study. To confirm the role of cationic charge in the ability of PEI-MWCNTs to induce cytokine and growth factor production, we also compared the cytokine production induced by PEI-MWCNTs, cc-PEI-MWCNTs, and unattached PEI polymer. As shown in Figure 3B, 24 h after the introduction of these agents, the polymer alone had no effect on cytokine or growth factor production, while the robust response to PEI-MWCNTs was significantly decreased after conversion to COOH in cc-PEI-MWCNTs. In addition, the generation of IL-1β, PDGF-AA, and TGF-β1 responses was dose-dependent (Figure S4B). These results confirm the importance of the cationic surface functionalization in cellular response generation.

Abundance of Cellular Uptake Determines Activation of the NLRP-3 Inflammasome. Because cellular uptake and bioprocessing of *f*-MWCNTs could determine the generation of the pro-fibrogenic factors, TEM and confocal Raman microscopy were used to examine the subcellular localization of *f*-MWCNTs in THP-1 and BEAS-2B cells.[25] Figure 4A and Figure S5A,B show the electron micrographs and confocal Raman spectra of cells incubated with the tubes for 24 h. The TEM images demonstrate that the tubes were taken up in both cell types in membrane-bound vesicles without impacting cell morphology or other intracellular organelles. Compared to AP-MWCNTs, the PEI-functionalized tubes were taken up with increased abundance, while NH_2 and sw-NH_2-MWCNTs showed the same and PEG- and COOH-MWCNTs reduced levels of uptake. Confocal Raman confirmed the characteristic D and G bands of MWCNTs in the exposed cells, indicating that the internalized *f*-MWCNTs are structurally intact (Figure 4A).

TEM and confocal Raman do not provide quantification of MWCNT uptake in cells. In order to more quantitatively assess cellular uptake, UV−vis spectrometry was performed by incubating THP-1 and BEAS-2B cells

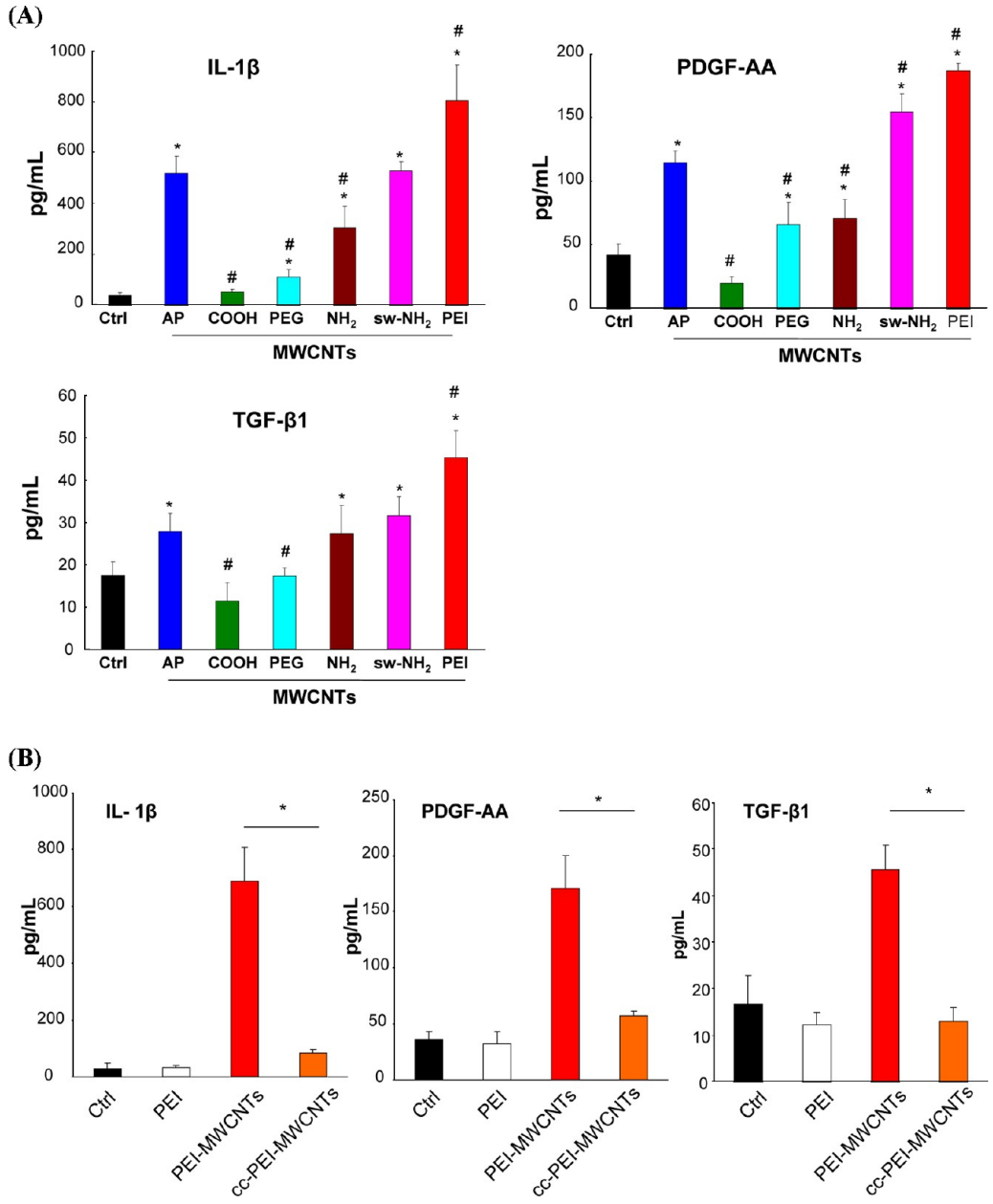

Figure 3. ***In vitro*** **pro-fibrogenic cytokines induced by** ***f*****-MWCNTs. (A) Cytokine production (IL-1**β**, TGF-**β**1, and PDGF-AA) induced by** ***f*****-MWCNTs. Cytokines were tested after cellular treatment with 60** μ**g/mL of the tubes at 37 °C for 24 h; *$p < 0.05$ compared to Ctrl, #$p < 0.05$ compared to AP-MWCNTs. (B) Comparison of cytokine production induced by PEI and cc-PEI-MWCNTs. After incubation with 120** μ**g/mL tubes for 24 h, cytokine production was determined by ELISA; *$p < 0.05$ compared to PEI-MWCNTs.**

with tubes for 3 h, washing the cells three times in PBS before sonication, and then studying tube absorbance in the lysates at 550 nm (Figure 4B). The absolute amounts of tube uptake were calculated by using standard absorbance curves for each tube type. PEI-MWCNT uptake values were ~29 and 18 pg/cell in THP-1 and BEAS-2B cells, respectively, which was significantly higher than the uptake of AP-MWCNTs. In contrast, PEG and COOH-MWCNTs were taken up in lower abundance while NH_2-MWCNTs showed the same level of uptake as AP-MWCNTs. While sw-NH_2-MWCNTs were taken up with similar abundance as the pristine tubes in THP-1, the former tube type was taken up in significantly higher amounts in BEAS-2B cells. These uptake values were to a large extent confirmed by the use of flow cytometry to assess the level of cellular side scattering of tube-treated cells (Figure S5C). The increase in CNT uptake leads to an increase in cellular granularity, which is reflected by the quantitative increase in side scattering.[41] The cellular uptake data correlated well with the IL-1β production, suggesting that the abundance of tube uptake plays a role in IL-1β production. This notion was confirmed by using cytochalasin D, an inhibitor of actin polymerization,[42] to demonstrate the reduced cellular uptake of tubes (Figure S5D) and the IL-1β production

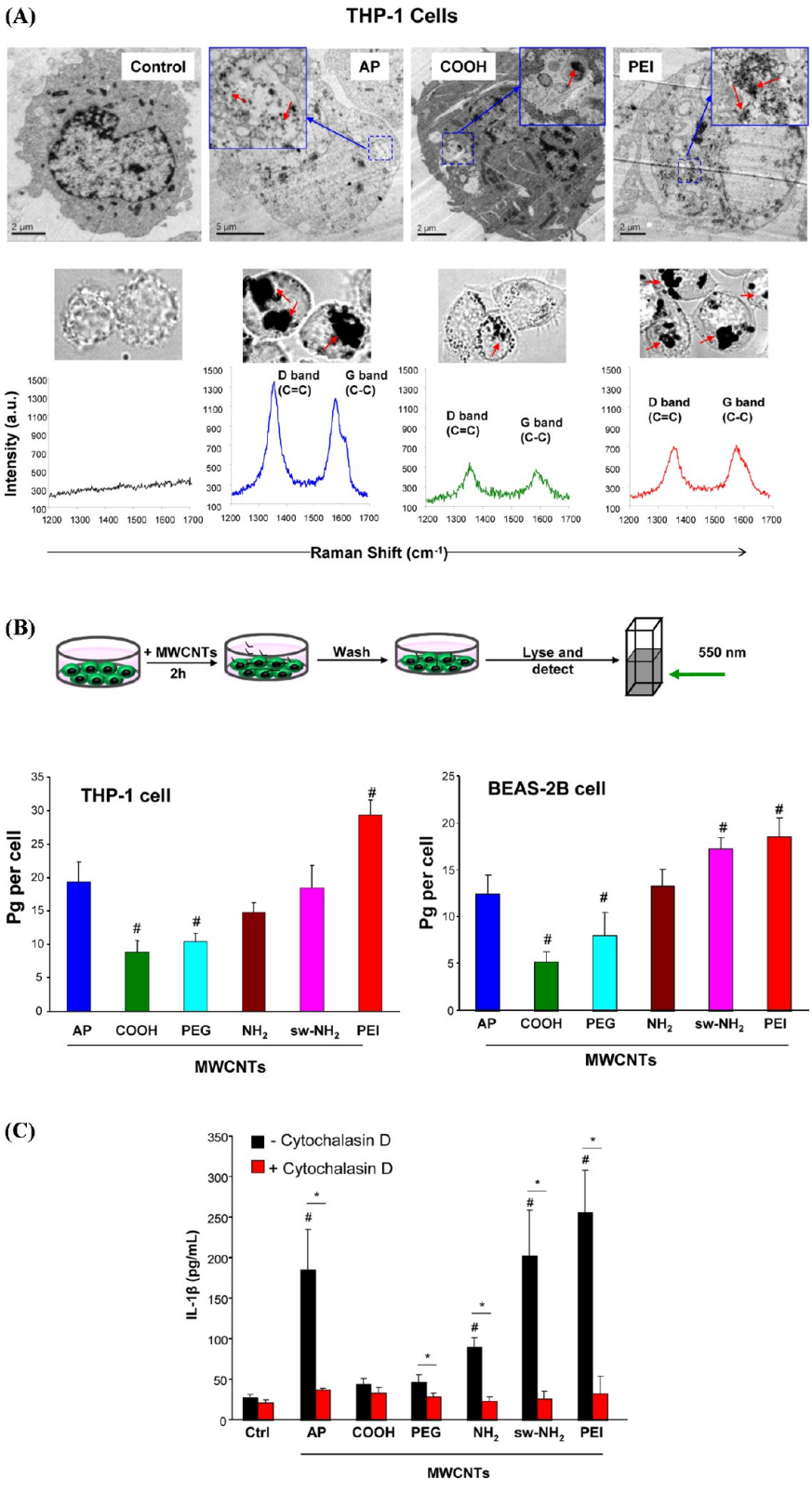

Figure 4. Cellular uptake of MWCNTs. (A) TEM images and Raman spectra of THP-1 cells treated with *f*-MWCNTs. The arrows in the TEM and light microscopy images show cellular uptake and localization of *f*-MWCNTs. Typical G and D bands on Raman spectra demonstrated the intact structure of tubes inside cells. (B) Quantification of MWCNTs associated with the cell. The schematic in the top panel shows the treatment of cells. The levels of MWCNTs associated with cells are shown in the lower panel. (C) IL-1β production in the presence of cytochalasin D. After pretreated for 3 h with 5 μg/mL cytochalasin D, THP-1 cells were incubated with 60 μg/mL MWCNTs for an additional 6 h; *$p < 0.05$ compared to tube only treated THP-1 cells, #$p < 0.05$ compared to AP-MWCNTs (B) or control (C).

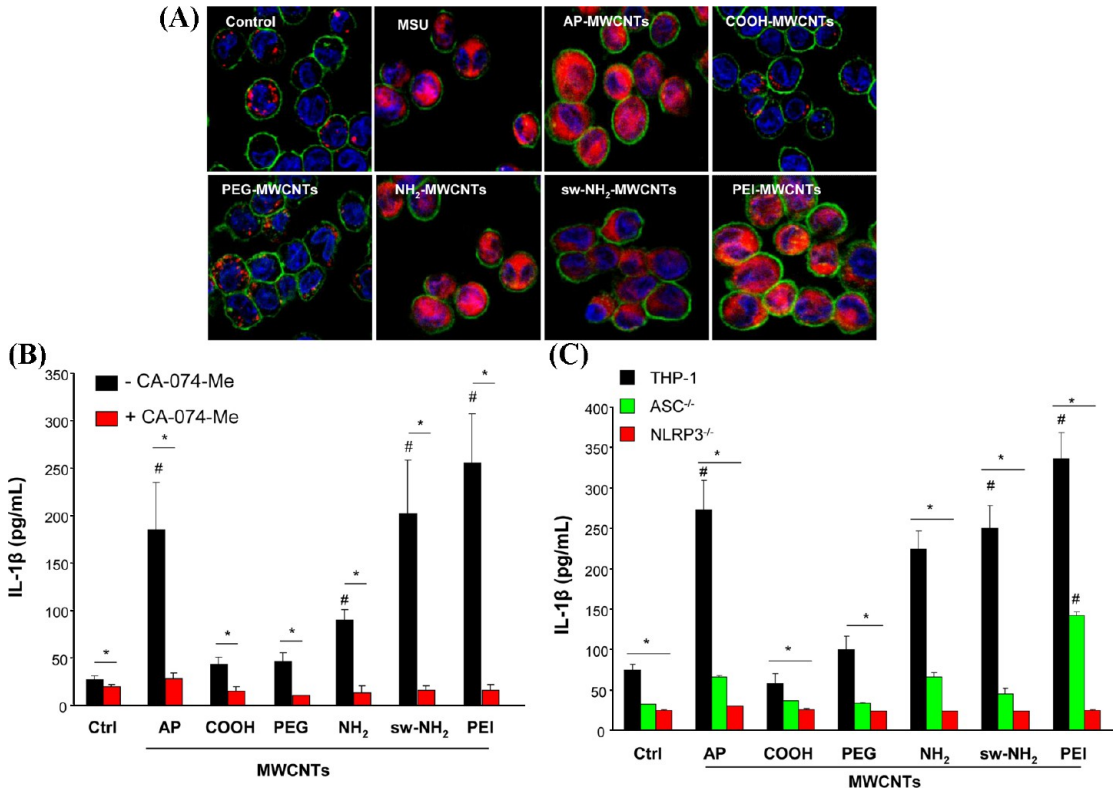

Figure 5. Lysosomal damage and cathepsin B release induced by the tubes. (A) Visualization of cathepsin B localization in THP-1 cells exposed to tubes. Lysosomal damage and cathepsin B release were identified by using Magic Red staining. THP-1 cells were seeded into 8-well chamber slides and incubated with *f*-MWCNTs at 120 μg/mL in complete RPMI 1640 for 3 h. After fixation, cells were stained with Magic Red (ImmunoChemistry Technologies), wheat germ agglutinin-Alexa 488, and Hoechst 33342 dye, followed by visualization under a confocal 1P/FCS inverted microscope. (B) IL-1β production in the presence of cathepsin B inhibitor, CA-074-Me. After pretreatment for 3 h with 50 μM CA-074-Me, THP-1 cells were incubated with 60 μg/mL MWCNTs for an additional 6 h. (C) IL-1β production in WT, NLRP3$^{-/-}$ and ASC$^{-/-}$ THP-1 cells. After incubation for 6 h, the IL-1β levels in the media of THP-1 wide-type or THP-1 knock down cells were examined by ELISA; *$p < 0.05$ compared to tube only treated THP-1 cells, #$p < 0.05$ compared to control.

induced by AP, PEG, NH_2, sw-NH_2, and PEI-MWCNTs in THP-1 cells (Figure 4C).

IL-1β production requires assembly of the NLRP3 inflammasome in macrophages.[43] NLRP3 activation by CNTs, monosodium urate (MSU), CeO_2 nanowires, and TiO_2 nanobelts is dependent on lysosome damage and cathepsin B release following the endocytosis of these long aspect ratio materials.[44] To assess lysosomal damage by *f*-MWCNTs, we used confocal fluorescence microscopy to study the containment of the lysosomal enzyme, cathepsin B, which can be detected by Magic Red in THP-1 cells.[45] As shown in Figure 5A, control cells showed a punctate distribution of the red Magic Red fluorescence in the intact lysosome, compared to the diffuse cytosolic release of cathepsin B in cells treated with monosodium urate (positive control). Interestingly, cells treated with COOH or PEG-MWCNTs showed a punctate distribution, which is in accordance with low levels of IL-1β production (Figure 3A). In contrast, AP, NH_2 sw-NH_2, and PEI-MWCNTs induced lysosomal damage, which is in agreement with higher levels of IL-1β production, as shown in Figure 3A. To demonstrate the importance of cathepsin B in NLRP3 inflammasome activation, THP-1 cells were treated with a cathepsin B inhibitor, CA-074-Me, before assessment of IL-1β production.[46] This demonstrated across-the-board reduction of IL-1β release in the cell culture media for all of the tubes capable of lysosomal damage (Figure 5B). Moreover, the involvement of NLRP3 inflammasome was confirmed by using NLRP3 and ASC gene knockout THP-1 cells, which exhibited significantly decreased IL-1β production compared to wild-type THP-1 cells after MWCNT treatment (Figure 5C). All considered, these data indicate that the IL-1β production is determined by the abundance of internalized MWCNTs, which further induce lysosomal damage and NLRP3 inflammasome activation.

***In Vivo* Validation of the Fibrogenic Potential of *f*-MWCNTs in the Lung.** In order to test the validity of the *in vitro* hazard ranking to pulmonary toxicity outcome, mice were exposed to *f*-MWCNTs by oropharyngeal installation, using a dose of 2 mg/kg, which has previously been shown to be on the steep part of the dose response curve for AP-MWCNTs and comparable to extrapolated occupational exposures.[24] First, we used confocal Raman microscopy to confirm that the tubes are taken up by pulmonary macrophages extracted from the bronchoalveolar lavage fluid (BALF) (Figure S6A). This

demonstrated the presence of the characteristic D and G bands of MWCNT structures for all tube types. We also demonstrated cathepsin B release in the lavage fluid macrophages from animals receiving MWCNT installation for 16 h before use of the animal BALF cells for *ex vivo* Magic Red staining. As demonstrated by the confocal images in Figure S6B, cathepsin B release could be demonstrated for all tube instillations except COOH-MWCNTs.

We also compared the extent of pulmonary inflammation in animals receiving tube installation for 40 h or 21 days. Animals receiving tube installation for 40 h showed significant increase in BALF IL-1β levels irrespective of the tube type (Figure S7). While most tubes also resulted in significant increases in PDGF-AA production, PEI-MWCNTs yielded the highest and COOH-MWCNTs the lowest levels for this growth factor. In contrast, the TGF-β1 levels in the BALF remained unchanged at 40 h. The differential cell counts in the BALF are shown in Figure S8A and demonstrate that all tubes could induce a significant increase in the neutrophil counts without intermaterial differences. While hematoxylin/eosin (H&E) staining demonstrated a small increase in the level of pulmonary inflammation for most tube types, PEI-MWCNTs induced slightly more effects (Figure S8B). Although the neutrophil count in the BALF was clearly reduced by 21 days (Figure S8C), histological examination showed the presence of chronic lung inflammation that was clearly exaggerated for PEI-MWCNTs and also more prominent in animals receiving NH_2 and sw-NH_2-MWCNT instillations (Figure S8D).

Assessment of fibrogenic effects in the lung was performed using ELISA to assess pro-fibrogenic growth factor levels in the BALF while also performing lung staining with Masson's trichrome and quantifying collagen content by the Sircol assay. Min-U-Sil (MUS) was used as positive control and AP-MWCNTs for comparison to *f*-MWCNTs. While MUS and AP-MWCNTs induced significant increases in TGF-β1 and PDGF-AA levels, COOH-MWCNTs failed to induce an increase, which, in turn, differs from the robust increase by PEI-MWCNTs (Figure 6). PEG, NH_2, and sw-NH_2-MWCNTs showed similar increases compared to AP-MWCNTs. IL-1β production is typically an early event during fibrogenesis,[46] and this effect decreases to background levels after 21 days after initial exposure of CNTs.[38] Consistent with these results, an increased production of IL-1β was observed at 40 h (Figure S7) but not at 21 days (Figure 6). However, there was no change in IL-1β production by 21 days.[24] Trichrome staining demonstrated significant increases in collagen deposition around the airways of AP-MWCNT-treated animals (Figure 7A). In contrast, carboxyl and PEG-functionalized tubes showed less collagen deposition, while PEI functionalization greatly enhanced this effect. The NH_2 and sw-NH_2-MWCNTs exhibited similar effects to AP-MWCNTs. Interestingly, while the presence of CNTs could be observed in pulmonary macrophages during staining of lung sections with Alcian Blue/PAS (Figure S9),[47] these were not the same areas in which collagen deposition could be seen to occur in the animal lung. Use of the Sircol assay confirmed a significant lung collagen deposition in animals exposed to PEI-MWCNTs compared to those exposed to AP-MWCNTs (Figure 7B). In contrast, COOH-MWCNTs and PEG-MWCNTs showed no significant increase in collagen deposition, while NH_2 and sw-NH_2-MWCNTs induced significant increases on par with AP-MWCNTs.

In order to confirm the pro-fibrogenic effects of the cationic surface in the exaggerated effects of PEI-MWCNTs, we also compared the effects to unattached PEI polymer and PEI-MWCNTs on which the amino groups were converted to COOH (cc-PEI-MWCNTs) at 21 days after oropharyngeal instillation. While the polymer itself did not trigger TGF-β1 and PDGF-AA production, its covalent attachment to the tube surface did increase the production of above growth factors compared to control animals (Figure 8A). In contrast, cc-PEI-MWCNTs showed a significant decrease in the levels of these growth factors. The findings were confirmed by the histology images (Figure 8B) and determination of the collagen content of the lungs (Figure 8C). This confirms the *in vivo* pro-fibrogenic effects of a strong cationic MWCNT surface.

DISCUSSION

In this study, syntheses of COOH, PEG, NH_2, sw-NH_2, and PEI-conjugated MWCNTs were used to investigate the role of surface functionalization and charge on the biological effects of *f*-MWCNTs using a predictive *in vitro*/*in vivo* toxicological approach. This demonstrated that PEI-MWCNTs induced significantly higher production of IL-1β and pro-fibrogenic growth factors, TGF-1β and PDGF-AA, *in vitro* and *in vivo*. Moreover, the differential IL-1β productions were shown to correlate with the differences in THP-1 uptake of the tubes, as well as their abilities to induce lysosomal injury and activation of the NLRP3 inflammasome. Similar effects on lysosome damage were seen in pulmonary macrophages obtained from the BALF of animals receiving oropharyngeal installation. These results are in agreement with the extent of chronic lung inflammation, fibrosis, and collagen deposition, toward which it was confirmed that PEI-MWCNTs induced the strongest effects, while NH_2 and sw-NH_2-MWCNTs exerted similar effects to AP-MWCNTs. In contrast, the effects of COOH and PEG-MWCNTs were reduced compared to the effects of AP-MWCNTs. These results demonstrate that pulmonary fibrogenic effects by *f*-MWCNTs are dependent on the attached surface groups as well as their charge. This is of considerable importance toward understanding the hierarchy of MWCNT properties that may contribute to their toxicological potential

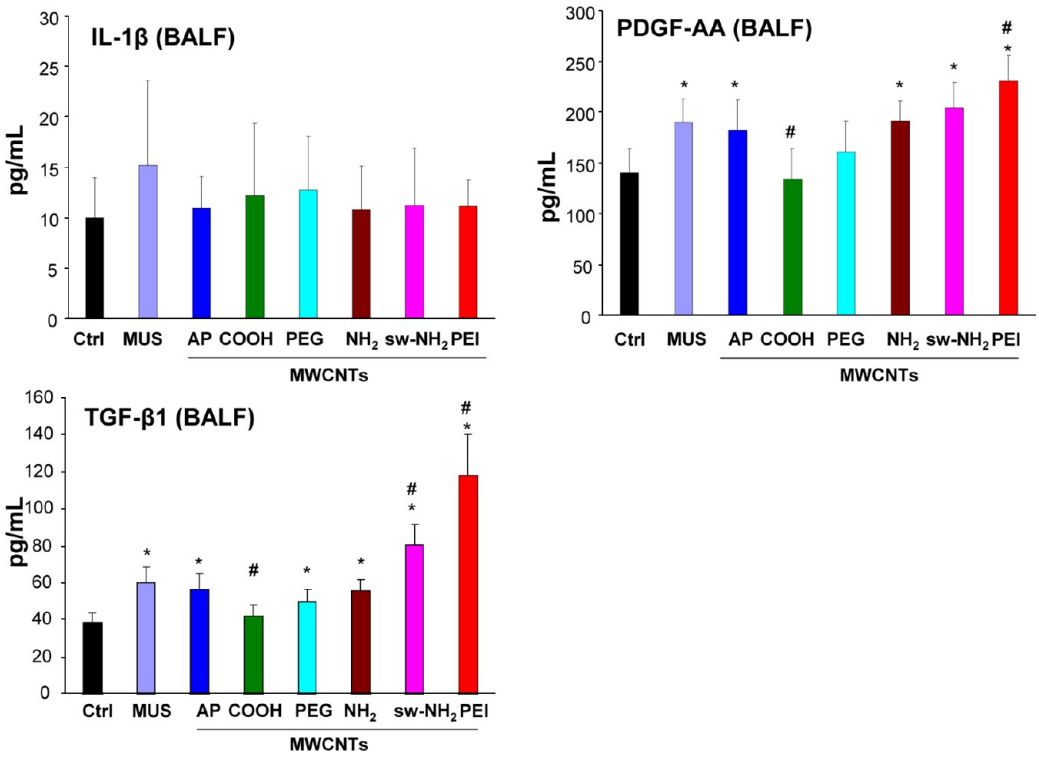

Figure 6. Cytokine production in BALF of animals after 21 d exposure to tubes. Tubes were oropharyngeally administrated at 2 mg/kg (6 mice in each group). After 21 days, animals were sacrificed to analyze IL-1β and growth factor production in BALF by ELISA. * $p < 0.05$ compared to Ctrl, # $p < 0.05$ compared to AP-MWCNTs.

other than the traditionally quoted fiber-like dimensions, which we do not observe in our study.

Functionalized CNTs are generally considered more biocompatible than pristine CNTs because of improved hydrophilicity and dispersion in biological media. This notion was supported by numerous *in vitro* studies looking at the cytotoxicity of *f*-MWCNTs as well as exploring the *in vivo* toxicological potential of COOH, taurine, polystyrene, and pluronic-functionalized MWCNTs.[21,24−27] However, most of the studies were performed with different starting materials, and we show here, for the first time, that systematic variation of functionalized groups on the same MWCNT surface can exert differential structure−activity relationships that hold true at cell and lung levels. Moreover, it is also possible to relate the surface charge of the *f*-MWCNTs to cellular uptake and triggering of lysosomal injury and inflammasome activation, which plays a role in the generation of pulmonary fibrosis. Previous studies have demonstrated the important role of inflammasome activation in inducing pulmonary inflammation and fibrosis.[48] This tends to be a relatively early response as exemplified by increased IL-1β production at 40 h (Figure S7), which subsequently declines and returns to background levels by 21 days.[49] However, the early phase of IL-1β production initiates a cascade of events that leads to downstream TGF-β1 and PDGF-AA production in epithelial and transitioning mesenchymal cells. This culminates in progressive collagen deposition and pulmonary fibrosis. Both the cellular and *in vivo* response outcomes suggest that the attachment of anionic COOH and PEG groups could act as safer design features that reduce the bioavailability and catalytic injury by MWCNTs. In contrast, neutral or weak cationic functionalization does not significantly change the fibrotic potential of AP-MWCNTs, while cationic PEI functionalization induced extensive lung fibrosis. This suggests that high cationic density should be avoided or charge neutralization should be considered as a safer design feature for cationic tubes. In addition to the toxicological effects of surface charge, the clearance rate of *f*-MWCNTs could play a role in determining their fibrogenic potential. This requires accurate quantitative techniques to determine the CNT clearance rate, which is not currently available.

Our results showed that COOH or PEG functionalization reduced the fibrotic potential of pristine tubes by lowering their bioavailability. This is likely due to the anionic charge, which leads to high suspension stability (~95% tubes remain in suspension in cell culture media by 20 h). This reduces tube sedimentation and cellular uptake as demonstrated by TEM images (Figure 4A), tube release into cellular lyses (Figure 4C), and side scatter studies (Figure S5C). In contrast, the close to neutral NH_2 and weak cationic sw-NH_2-MWCNTs show similar fibrogenic potential as AP-MWCNTs, probably because the low surface coverage (<1.5%) maintains a relatively hydrophobic surface. This makes the tubes less stable in physiological media and in the lysosomes, allowing them to come out of solution and make contact with the lysosomal membrane.

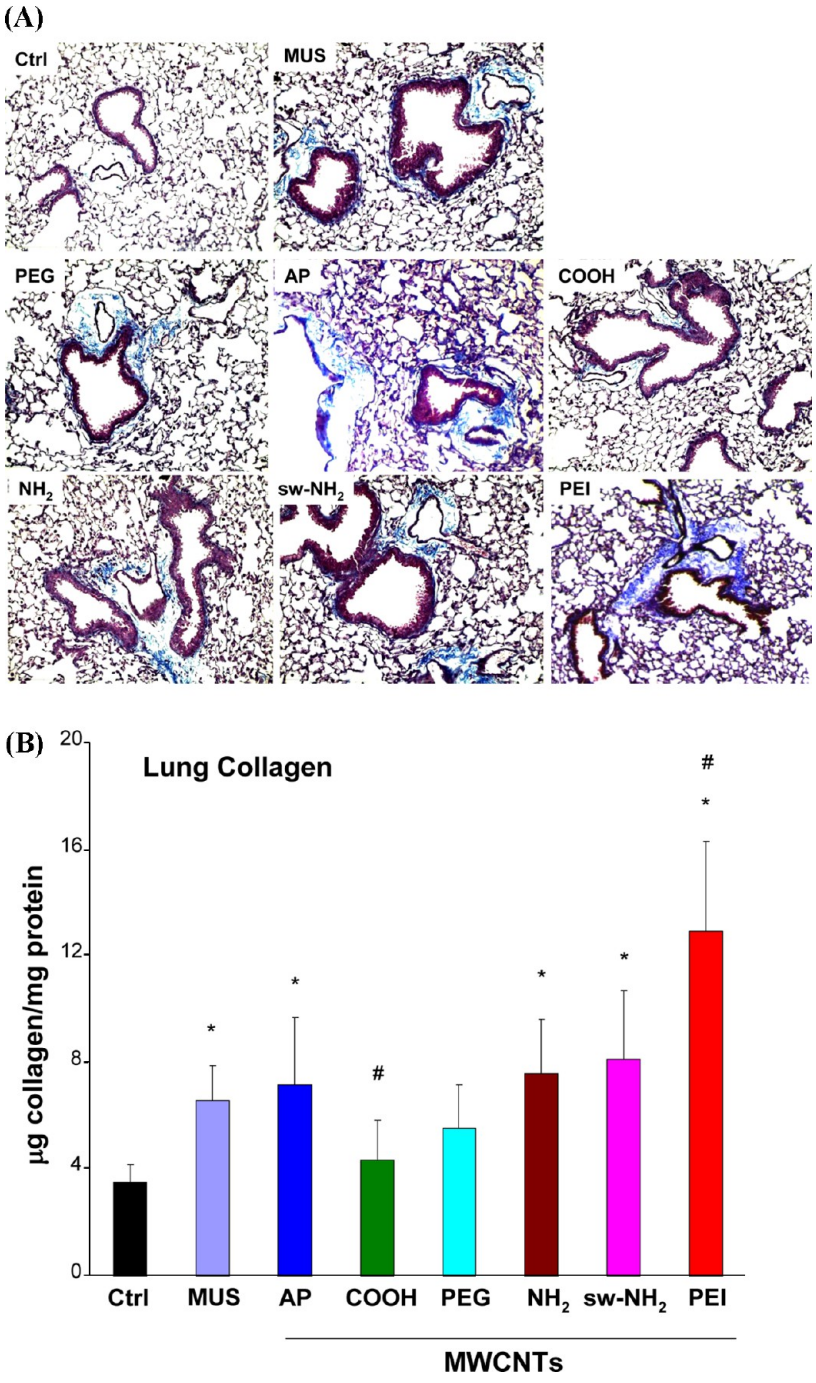

Figure 7. Pulmonary fibrosis induced by *f*-MWCNTs. (A) Trichrome staining to determine lung fibrosis after 21 days exposure to tubes. (B) Quantification of collagen in lung tissues after 21 day exposure to tubes; *$p < 0.05$ compared to control, #$p < 0.05$ compared to AP-MWCNTs.

Injury to the membrane and cathepsin B release leads to NLRP3 inflammasome activation. The most interesting impact is the effect of PEI-MWCNTs, widely used in sensors,[50] nanocomposites,[51] intracellular carrier,[17] sorbent,[52] *etc.* These tubes induce not only robust IL-1β, TGF-β1, and PDGF-AA production *in vitro* and in the intact lung but also chronic pulmonary fibrosis. The most likely explanation for this outcome is that PEI-MWCNTs had the lowest suspension stability and are thus more likely to settle at the bottom of the wells, where they make more cellular contact. The positive charge on the tube surface may also enhance cellular uptake because of increased binding to anionic groups on the cell surface.[53] Finally, following tube uptake into the lysosome, the PEI groups on the poorly suspended tubes may lead to direct interactions with and damage to the lysosomal membrane, in addition to inducing osmotic swelling of this organelle due to a proton sponge effect.[29,33]

The possible relevance of the predictive toxicological paradigm to pulmonary damage in humans needs

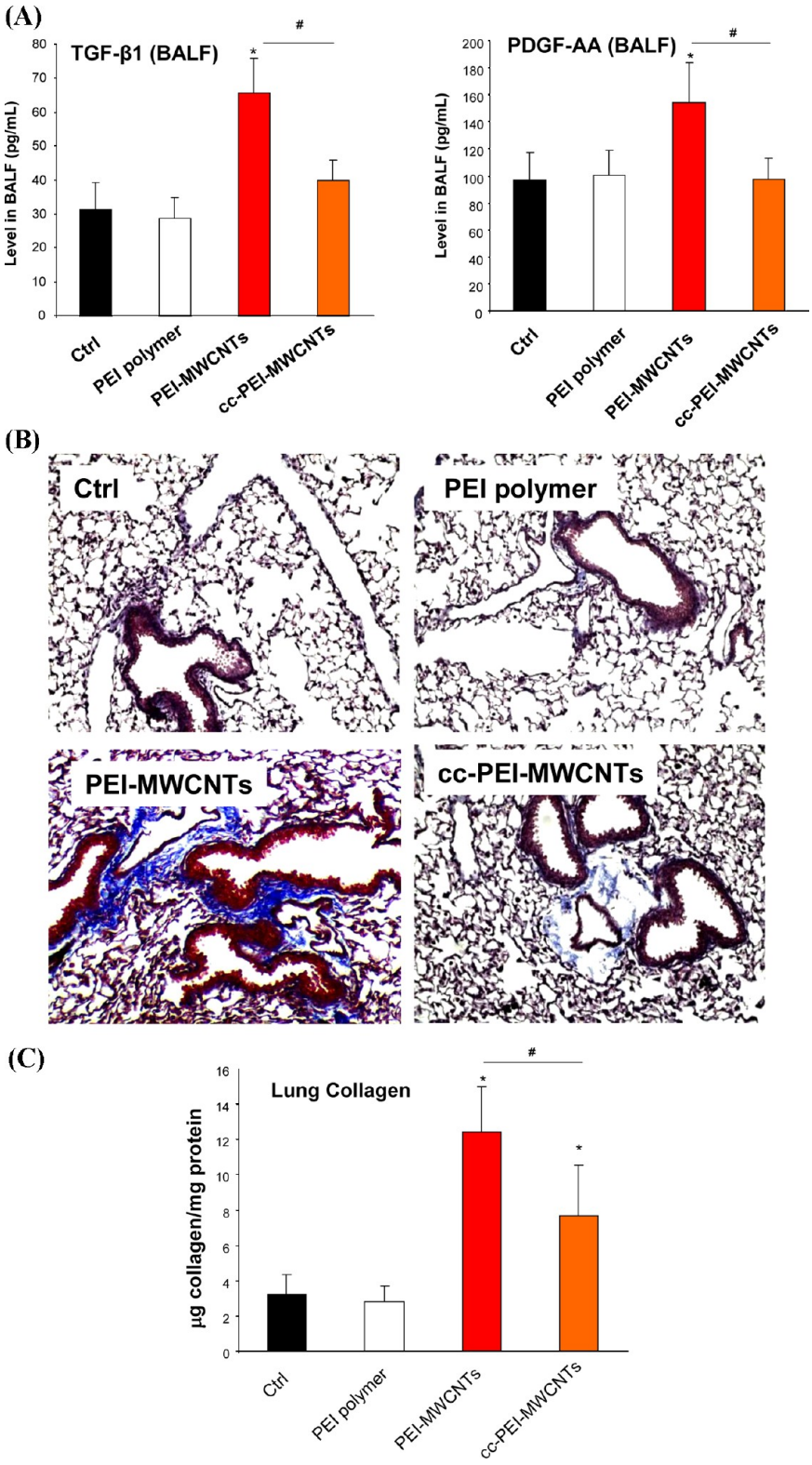

Figure 8. Carboxyl-converted PEI-MWCNTs show decreased lung fibrosis. (A) TGF-β1 and PDGF-AA level in BALF. (B) Trichrome staining of lung tissues. (C) Six mice were included in each group. Total collagen content in the lungs of animals after 21 days exposure; *$p < 0.05$ compared to control, #$p < 0.05$ compared to PEI-MWCNTs.

to consider real life exposure scenarios in the workplace. While we were not able to include human exposures in our study, several recent studies have shown that when the lung burden and state of CNT dispersion are kept similar, pulmonary responses to bolus exposure (such as oropharyngeal instillation) are comparable to short-term inhalation exposures in rodents which, in turn, can be reconciled with the lung

burdens during inhalation exposure in humans.[54,55] In order to extrapolate the doses used in our animal exposures to MWCNT exposure in human, we used reported data[56] showing that the airborne levels of MWCNTs to which humans can be exposed in a research facility could be as high as 400 $\mu g/m^3$. In addition, NIOSH has proposed a recommended limit of exposure as 7 $\mu g/m^3$ for CNTs. Using the calculation approach being used at NIOSH,[57] we could estimate that a worker exposure of 400 $\mu g/m^3$ for 8 h/day over a five month time period over a 45 years working lifetime could lead to a lung burden similar to a bolus exposure of 2 mg/kg in the mouse.[58] It is also important to know the relevance of *in vitro* dose to *in vivo* dosimetry. We used lung alveolar epithelium surface area to calculate the CNT exposure levels to cells. The mouse experiment was performed at 2 mg/kg, which is equivalent to 1 mg/m^2 of MWCNT exposure in the mouse lung, assuming the alveolar epithelium surface area of 0.05 m^2 and a body weight of 25 g.[59] Assuming that the *in vitro* MWCNT dose is homogeneously distributed in the tissue culture dish and the thickness of cell layer being 10 μm, the *in vitro* cell exposure dose would be 100 $\mu g/mL$. The dose range we used for *in vitro* assay is from 30 to 120 $\mu g/mL$, which is comparable to the dose in the mouse experiment. These estimates suggest that the MWCNT doses tested in cells and mice in this study are comparable to occupational exposures in humans. However, this *in vitro* dosage is only an estimation based on several assumptions, and the ISDD model[60] and more sensitive measurements for CNTs may be needed to better estimate the *in vitro* exposure dose.

Because animal experiments are laborious, costly, and time-consuming, it is advantageous to develop predictive toxicological approaches that use cellular studies to gain an understanding of the toxicological mechanisms and structure–activity relationships before performing targeted animal experiments. Our demonstration of a predictive toxicological paradigm to investigate the fibrotic potential of surface-functionalized MWCNTs by using cell types that play a role in the pathophysiology of fibrosis in the lung serves as an example of how future studies can be performed to compare multiple materials in a single round of experimentation. Considering the increasing number of CNTs with various functionalizations emerging in the marketplace, this predictive paradigm has the potential to increase the speed and accuracy of lung toxicity screening for regulatory decision making as well as the safer design of CNTs for commercial use and biomedicine. One immediate consideration could be to use the different surface functionalization categories to group CNTs or to provide read-across, which represents a process where end point information for one CNT may be used to predict the same end point for another CNT based upon similarities in their chemical structure or functionality.

CONCLUSION

We showed the role of surface charge in determining the pulmonary fibrogenic effects of MWCNTs. While anionic functionalization (COOH and PEG) decreases the pulmonary fibrogenic potential compared to AP-MWCNTs, strong cationic functionalization (PEI) induces more pulmonary fibrosis. Neutral (NH_2) and weak cationic (sw-NH_2) functionalized tubes have similar fibrogenic potential compared to pristine tubes. The mechanism of these effects involves differences in cellular uptake of MWCNTs, lysosomal damage, cathepsin B release, as well as NLRP3 inflammasome activation. These constitute *in vitro* assessment methods that can be used for hazard ranking and therefore highly relevant to prioritizing targeted animal experiments. This predictive approach to MWCNT safety evaluation can be used for regulatory decision making as well as safer design of CNTs.

MATERIALS AND METHODS

Carbon Nanotubes and Chemicals. Raw or as-prepared MWCNTs (AP-MWCNTs) in powder form were purchased from Cheap Tubes Inc. (Brattleboro, VT, USA). Dipalmitoylphosphatidylcholine (DPPC), hexane, polyethylene glycol (PEG), polyethyleneimine (PEI), CA-074-Me, and cytochalasin D were purchased from Sigma-Aldrich (St. Louis, MO, USA). N-Boc-amino acid was kindly provided by Prof. Prato at University of Trieste, Italy. Min-U-Sil was obtained from U.S. Silica (Frederick, MD, USA). Bronchial epithelial growth medium (BEGM) was obtained from Lonza (Mapleton, IL, USA), which is supplemented with a number of growth factors, including bovine pituitary extract (BPE), insulin, hydrocortisone, hEGF, epinephrine, triiodothyronine, transferrin, gentamicin/amphotericin-B, and retinoic acid. Roswell Park Memorial Institute medium 1640 (RPMI 1640) was purchased from Invitrogen (Carlsbad, CA, USA). Low-endotoxin bovine serum albumin (BSA) and fetal bovine serum (FBS) were from Gemini Bio-Products (West Sacramento, CA, USA).

Syntheses of *f*-MWCNTs. COOH and sw-NH_2-MWCNTs were synthesized from AP-MWCNTs, while PEG, NH_2, and PEI-MWCNTs were derivatives of COOH-MWCNTs. In a typical COOH-MWCNT synthesis, 1 g of AP-MWCNTs was added into 120 mL of concentrated HNO_3 and H_2SO_4 (1:3, v/v) solution at 120 °C in an oil bath to react while stirring for 30 min.[8] After 10-fold dilution with deionized water (DI H_2O), the suspension was filtered through a 0.45 μm PTFE membrane, washed with DI H_2O to a neutral pH, and vacuum-dried at 70 °C. For sw-NH_2-MWCNT synthesis, AP-MWCNTs (20 mg) were dispersed in DMF (dry, 10 mL) by sonication for 2 min. N-Boc-amino acid (31 mg, 0.10 mM) and paraformaldehyde (48 mg, 0.10 mM) with DMF (dry, 5 mL) were added to the suspension, and the reaction mixture was refluxed at 120–130 °C for 96 h.[18] After that, the reaction mixture was cooled to room temperature and centrifuged at 3500 rpm for 5 min. The supernatant was discarded, and the tubes were treated with 10 mL of 0.1 M HCl for 2 h to remove Boc. The tubes were separated by centrifugation, washed in methanol 5 times, and dried for further use as sw-NH_2-MWCNTs. For preparation of PEG, NH_2, and PEI-MWCNTs, 150 mg of COOH-MWCNTs was dissolved in 75 mL of dry DMF, following which the suspension was sonicated for 5 min and 30 mL of $SOCl_2$ was added gradually in an ice-bath to acylate the COOH group. After 24 h reflux at 120 °C with magnetic stirring, the reaction mixture was centrifuged at 10 000 rpm. The pellets were washed with anhydrous THF, dried under vacuum at room temperature for 2 h, and

then resuspended into 75 mL of DMF. The suspension was equally divided into three flasks. After magnetically stirring under nitrogen atmosphere at 90 °C for 1 h, 500 mg of PEG, hexane diamine, or PEI was added into each flask and reacted with acylated COOH-MWCNTs for 3 days. Subsequently, the reaction mixtures were centrifuged, washed with methanol, and dried at 70 °C. The resulting solid powders contained PEG, NH_2, and PEI-MWCNTs. To prepare cc-PEI-MWCNTs, amine groups on the PEI-MWCNTs were converted to carboxylates by succinic anhydride. Briefly, 150 mg of succinic anhydride was dissolved in 50 mL of a pH 9.2 carbonate buffer, and 5 mg of PEI-MWCNTs was added to the buffered solution, which was stirred for 48 h at room temperature.[29] The mixture was then centrifuged, washed with ethanol (3×) and water (3×), and resuspended in water for later use.

Physicochemical Characterization of MWCNTs. TEM (JEOL 1200 EX, accelerating voltage 80 kV) was used to observe the size, length, and structure of the *f*-MWCNTs. TEM samples were prepared by suspending 50 μg/mL of MWCNTs in DI H_2O, placing a drop of the MWCNT suspension on the grids, and leaving it air-dry at room temperature. For XPS detection, tubes were suspended in water, dropped onto a silicon wafer, and the air-dried tube sheets were tested on X-ray photoelectron spectroscopy (XPS, Omicron, MA) to identify the elemental composition on the surface of the tubes. Fourier transformed infrared (FTIR) spectra were obtained with a Bruker Vertex 70 instrument. All of the samples were prepared as pellets using spectroscopic grade KBr. Dynamic light scattering and analysis of zeta-potential (Brookhaven Instruments Corporation, Holtsville, NY) was performed to determine the hydrodynamic tube diameter and surface charge in water, cell culture media, and PBS, as previously described by us.[35,61] We have previously demonstrated that the metal content of the AP-MWCNTs was 5.25 wt % and decreased to 1.88 wt % after acid treatment.[24]

Preparation of MWCNT Suspensions in Media. MWCNTs were weighed on an analytical balance in a fume hood and suspended in distilled, deionized H_2O at a concentration of 2 mg/mL. These suspensions were sonicated at 100 W output with frequency of 42 kHz for 15 min in a water sonicator (Branson, Danbury, CT, USA, model 2510). The suspensions were used as stock solutions for further dispersion in cell culture media or PBS. An appropriate amount of each stock solution was added to cell culture media or PBS to achieve the desired final concentration. For better dispersion, BSA and DPPC were added to BEGM medium or PBS at 0.6 and 0.01 mg/mL, before the addition of *f*-MWCNTs as reported by us.[35] The diluted tube suspensions were dispersed using a sonication probe (Sonics & Materials, USA) at 32 W for 15 s at the desired final concentration before further use.

Cellular Culture and Coincubation with MWCNTs. BEAS-2B and THP-1 cells were obtained from ATCC (Manassas, VA). BEAS-2B and THP-1 cells were cultured in BEGM and RPMI 1640 medium supplemented with 10% fetal bovine serum, respectively, at 5% CO_2 and 37 °C. Before exposure to *f*-MWCNTs, BEAS-2B cells were seeded at a density of 5×10^3/well in 96-well plates (Corning, NY, USA) at 37 °C overnight. All the *f*-MWCNT solutions were freshly prepared in BEGM containing 0.6 mg/mL BSA plus 0.01 mg/mL DPPC before addition to the BEAS-2B cells. *f*-MWCNTs were suspended in complete RPMI 1640 medium supplemented with 10% fetal bovine serum and 10 ng/mL LPS to treat THP-1 cells. For THP-1 cells, they need to be primed for IL-1β production. Briefly, aliquots of 5×10^4 THP-1 cells were seeded in 0.1 mL complete medium with 1 μg/mL phorbol 12-myristate acetate (PMA) overnight in 96-well plates (Corning, NY, USA). The cells were primed with 10 ng/mL lipopolysaccharide (LPS) to initiate transcriptional activation of the IL-1β promoter. After exposure to tubes, IL-1β was detected in culture medium using human or mouse IL-1β ELISA kits.

Coculture of THP-1 and BEAS-2B Cells. Cellular coculture was performed using Corning HTS Transwell-96 system with 1.0 μm pore size (Corning, NY, USA) to detect TGF-β1 and PDGF-AA productions. THP-1 cells (1×10^4) were seeded into the upper chamber of a transwell system. BEAS-2B cells (5×10^3) were seeded in the lower chamber. After overnight incubation of each chamber separately, upper and lower chambers were assembled together, both THP-1 and BEAS-2B cells were exposed to the tubes suspended in BEGM medium for 24 h, then the supernatant was collected and used to measure active TGF-β1 and PDGF-AA by TGFβ1 Emax ImmunoAssay Systems (Promega, WI, USA) and human/mouse PDGF-AA Quantikine ELISA kit (R&D, MN, USA), respectively.

Detection of Cellular Uptake by TEM. After exposure to MWCNTs for 24 h, the cells were washed and fixed with 2% glutaraldehyde in PBS. After post-fixation in 1% osmium tetroxide in PBS for 1 h, the cells were dehydrated in a graded series of ethanol, treated with propylene oxide, and embedded in Epon. Approximately 50−70 nm thick sections were cut on a Reichert-Jung Ultracut E ultramicrotome and picked up on Formvar-coated copper grids. The sections were stained with uranyl acetate and Reynolds lead citrate and examined on a JEOL transmission electron microscope at 80 kV in the UCLA BRI Electron Microscopy Core as previously reported.[25]

Quantification of MWCNTs in Cells. THP-1 or BEAS-2B cells were seeded in 6-well plates for overnight incubation. Both cell types were exposed to 120 μg/mL tubes for 3 h and then washed in PBS three times to eliminate the residual free MWCNTs. Cell samples were finally resuspended in 500 μL of PBS and lysed using a sonication probe. The UV−vis absorbance of cell lyses was measured at 550 nm. The concentration of MWCNTs in cell lyses was determined by using standard curves of concentration *versus* absorbance produced, and the cellular uptake of MWCNTs could be calculated by the following formula: $U = (f_i(A_i - A_0) \times V_i)/(N_i)$, where U represents cellular uptake level of MWCNTs, $f_i(A_i - A_0)$ is the standard curve equation of tubes, N_i is the cell number before cell lyses, V_i is the volume of cell lyses solution, A_i and A_0 are the absorbance of tube-treated and untreated cell lyses, respectively.

Animal Treatment and Assessment of Exposure Outcomes. Eight-week-old male C57Bl/6 mice purchased from Charles River Laboratories (Hollister, CA) were used for animal experiments. All animals were housed under standard laboratory conditions that have been set up according to UCLA guidelines for care and treatment of laboratory animals as well as the NIH Guide for the Care and Use of Laboratory Animals in Research (DHEW78-23). These conditions are approved by the Chancellor's Animal Research Committee at UCLA and include standard operating procedures for animal housing (filter-topped cages; room temperature at 23 ± 2 °C; 60% relative humidity; 12 h light, 12 h dark cycle) and hygiene status (autoclaved food and acidified water). Animal exposure to tubes was carried out by an oropharyngeal aspiration method as described by us.[25] In detail, the animals were anesthetized by intraperitoneal injection of ketamine (100 mg/kg)/xylazine (10 mg/kg) in a total volume of 100 μL. The anesthetized animals were held in a vertical position. Fifty microliter aliquots of MWCNT suspension in PBS were instilled at the back of the tongue to allow pulmonary aspiration with a final dose at 2 mg/kg. Each experiment included control animals receiving the same volume of PBS with BSA (0.6 mg/mL) and DPPC (0.01 mg/mL). The positive control group in each experiment received 5 mg/kg crystalline silica in the form of quartz particles (Min-U-Sil). The mice were sacrificed after 40 h or 21 days. BALF and lung tissue were collected as previously described.[24] The BALF was used for performance of total and differential cell counts and measurement of IL-1β, TGF-β1, and PDGF-AA levels. Lung tissue was stained with hematoxylin/eosin or with Masson's Trichrome stain and was homogenenized with a Tissuemiser homogenizer (Fisher Scientific) for the assessment of total collagen production (Sircol Collagen Assay, UK).

Visualization of Cathepsin B Localization by Confocal Microscopy. Cathepsin B was detected in THP-1 cells or primary alveolar macrophages extracted from BALF using Magic Red−cathepsin B substrate. For cell treatment, THP-1 cells were treated with 120 μg/mL *f*-MWCNTs in c-RPMI 1640 for 3 h, while primary alveolar macrophages were collected from the BALF of mice exposed to tubes for 16 h and incubate in an 8-well chamber for 2 h. The cell samples were then washed with PBS, stained with Magic Red (ImmunoChemistry Technologies) in PBS for 1 h, and fixed in 4% paraformaldehyde for 20 min. Following washes by PBS twice, cell membrane and nucleus were stained with AlexaFluor488-conjugated wheat germ agglutinin (WGA) and Hoechst 33342, respectively, in PBS at room temperature for 1 h.[25] The cells were visualized under a confocal microscope (Leica Confocal SP2 1P/FCS) in the UCLA/CNSI

Advanced Light Microscopy/Spectroscopy Shared Facility. High-magnification images were obtained with the 63× objective. Cells without MWCNT treatment were used as control. Cells treated with 100 μg/mL of MSU were used as the positive control.

Sircol Assay for Total Collagen Production. The right cranial lobe of each lung was suspended in PBS at around 50 mg tissues/mL and homogenized for 60 s with a tissue homogenizer (Fisher Scientific). Triton X-100 was added at a 1% concentration, and the samples were incubated for 18 h at room temperature. Acetic acid was added to each sample to a final concentration of 0.5 M and incubated at room temperature for 90 min. Cellular debris was pelleted by centrifugation and the supernatant analyzed for total protein, using a BCA assay kit (Pierce/Thermo Fisher Scientific) according to manufacturer's instructions. The Sircol soluble collagen assay kit (Biocolor Ltd., Carrickfergus, UK) was used to extract collagen from duplicate samples using 200 μL of supernatant and 800 μL of Sircol dye reagent according to the manufacturer's instructions. Similarly prepared collagen standards (10−50 μg) were run in parallel. Collagen pellets were washed twice with denatured alcohol and dried before suspended in alkali reagent. Absorbance at 540 nm was measured on a plate reader (SpectroMax M5e, Molecular Devices Corp., Sunnyvale, CA). Data were expressed as micrograms of soluble collagen per milligram of total protein.

Confocal Raman Microscopy. Raman analysis was performed using backscattering geometry in a confocal configuration at room temperature in a Renishaw inVia Raman microscope system equipped with a 514.5 nm Ar laser. Laser power and beam size were approximately 2.5 mW and 1 μm, respectively, while the integration time was adjusted to 15 s. For cell sample preparation, BEAS-2B or THP-1 cells were cultured on sterile glass coverslips overnight and then exposed to *f*-MWCNTs for 24 h. Cells were washed three times in PBS and fixed with 4% paraformaldehyde in PBS for 30 min before used for Raman analysis. For scanning of primary alveolar macrophages extracted from BALF of mice 40 h after exposure to tubes, primary macrophages were suspended in c-RPMI 1640 medium and seeded onto sterile glass coverslips. After 2 h incubation, cells were washed, fixed in 4% paraformaldehyde, and scanned under the confocal Raman microscope.

Statistical Analysis. Mean and standard deviation (SD) were calculated for each parameter. Results were expressed as mean ± SD of multiple determinations. Comparisons between groups were evaluated by two-side Student's *t* test or one-way ANOVA. A statistically significant difference was assumed to exist when p was <0.05.

Conflict of Interest: The authors declare no competing financial interest.

Acknowledgment. This work is supported by the U.S. Public Health Service Grants (U19 ES019528 and R01 ES016746). Infrastructure Support was also provided by National Science Foundation and the Environmental Protection Agency under Cooperative Agreement Number, DBI 0830117. Any opinions, findings, conclusions or recommendations expressed herein are those of the authors and do not necessarily reflect the views of the National Science Foundation or the Environmental Protection Agency. This work has not been subjected to an EPA peer and policy review. The findings and conclusions in this article are those of the authors and do not necessarily represent the views of the National Institute for Occupational Safety and Health. Prof. Prato at University of Trieste kindly provided us the N-Boc-amino acid used for the preparation of sw-NH_2-MWCNTs.

Supporting Information Available: TEM and FTIR of cc-PEI-MWCNTs, suspension stability, cytoxicity, dose response, *in vitro/in vivo* cellular uptake, *in vivo* cytokine production at 40 h, neutrophil count, H&E staining, and Alcian Blue/PAS staining. This material is available free of charge *via* the Internet at http://pubs.acs.org.

REFERENCES AND NOTES

1. Schnorr, J. M.; Swager, T. M. Emerging Applications of Carbon Nanotubes. *Chem. Mater.* **2011**, *23*, 646–657.
2. Wu, H. C.; Chang, X. L.; Liu, L.; Zhao, F.; Zhao, Y. L. Chemistry of Carbon Nanotubes in Biomedical Applications. *J. Mater. Chem.* **2010**, *20*, 1036–1052.
3. Tasis, D.; Tagmatarchis, N.; Bianco, A.; Prato, M. Chemistry of Carbon Nanotubes. *Chem. Rev.* **2006**, *106*, 1105–1136.
4. Liu, W. B.; Pei, S. F.; Du, J. H.; Liu, B. L.; Gao, L. B.; Su, Y.; Liu, C.; Cheng, H. M. Additive-Free Dispersion of Single-Walled Carbon Nanotubes and Its Application for Transparent Conductive Films. *Adv. Funct. Mater.* **2011**, *21*, 2330–2337.
5. Vairavapandian, D.; Vichchulada, P.; Lay, M. D. Preparation and Modification of Carbon Nanotubes: Review of Recent Advances and Applications in Catalysis and Sensing. *Anal. Chim. Acta* **2008**, *626*, 119–129.
6. Kauffman, D. R.; Star, A. Carbon Nanotube Gas and Vapor Sensors. *Angew. Chem., Int. Ed.* **2008**, *47*, 6550–6570.
7. Upadhyayula, V. K. K.; Deng, S. G.; Mitchell, M. C.; Smith, G. B. Application of Carbon Nanotube Technology for Removal of Contaminants in Drinking Water: A Review. *Sci. Total Environ.* **2009**, *408*, 1–13.
8. Li, R. B.; Wu, R.; Zhao, L.; Wu, M. H.; Yang, L.; Zou, H. F. P-Glycoprotein Antibody Functionalized Carbon Nanotube Overcomes the Multidrug Resistance of Human Leukemia Cells. *ACS Nano* **2010**, *4*, 1399–1408.
9. Li, R. B.; Wu, R. A.; Zhao, L. A.; Hu, Z. Y.; Guo, S. J.; Pan, X. L.; Zou, H. F. Folate and Iron Difunctionalized Multiwall Carbon Nanotubes as Dual-Targeted Drug Nanocarrier to Cancer Cells. *Carbon* **2011**, *49*, 1797–1805.
10. Saha, M. S.; Kundu, A. Functionalizing Carbon Nanotubes for Proton Exchange Membrane Fuel Cells Electrode. *J. Power Sources* **2010**, *195*, 6255–6261.
11. Kostarelos, K.; Bianco, A.; Prato, M. Promises, Facts and Challenges for Carbon Nanotubes in Imaging and Therapeutics. *Nat. Nanotechnol.* **2009**, *4*, 627–633.
12. Liu, J.; Rinzler, A. G.; Dai, H. J.; Hafner, J. H.; Bradley, R. K.; Boul, P. J.; Lu, A.; Iverson, T.; Shelimov, K.; Huffman, C. B.; *et al.* Fullerene Pipes. *Science* **1998**, *280*, 1253–1256.
13. Rahimpour, A.; Jahanshahi, M.; Khalili, S.; Mollahosseini, A.; Zirepour, A.; Rajaeian, B. Novel Functionalized Carbon Nanotubes for Improving the Surface Properties and Performance of Polyethersulfone (PES) Membrane. *Desalination* **2012**, *286*, 99–107.
14. Niu, L.; Luo, Y. L.; Li, Z. Q. A Highly Selective Chemical Gas Sensor Based on Functionalization of Multi-Walled Carbon Nanotubes with Poly(ethylene glycol). *Sens. Actuators, B* **2007**, *126*, 361–367.
15. Foillard, S.; Zuber, G.; Doris, E. Polyethylenimine-Carbon Nanotube Nanohybrids for SiRNA-Mediated Gene Silencing at Cellular Level. *Nanoscale* **2011**, *3*, 1461–1464.
16. Liu, M.; Chen, B.; Xue, Y. A.; Huang, J.; Zhang, L. M.; Huang, S. W.; Li, Q. W.; Zhang, Z. J. Polyamidoamine-Grafted Multiwalled Carbon Nanotubes for Gene Delivery: Synthesis, Transfection and Intracellular Trafficking. *Bioconjugate Chem.* **2011**, *22*, 2237–2243.
17. Varkouhi, A. K.; Foillard, S.; Lammers, T.; Schiffelers, R. M.; Doris, E.; Hennink, W. E.; Storm, G. Sirna Delivery with Functionalized Carbon Nanotubes. *Int. J. Pharm.* **2011**, *416*, 419–425.
18. Georgakilas, V.; Kordatos, K.; Prato, M.; Guldi, D. M.; Holzinger, M.; Hirsch, A. Organic Functionalization of Carbon Nanotubes. *J. Am. Chem. Soc.* **2002**, *124*, 760–761.
19. Hong, S. Y.; Tobias, G.; Al-Jamal, K. T.; Ballesteros, B.; Ali-Boucetta, H.; Lozano-Perez, S.; Nellist, P. D.; Sim, R. B.; Finucane, C.; Mather, S. J.; *et al.* Filled and Glycosylated Carbon Nanotubes for *In Vivo* Radioemitter Localization and Imaging. *Nat. Mater.* **2010**, *9*, 485–490.
20. Wu, W.; Wieckowski, S.; Pastorin, G.; Benincasa, M.; Klumpp, C.; Briand, J. P.; Gennaro, R.; Prato, M.; Bianco, A. Targeted Delivery of Amphotericin B to Cells by Using Functionalized Carbon Nanotubes. *Angew. Chem., Int. Ed.* **2005**, *44*, 6358–6362.
21. Vardharajula, S.; Ali, S. Z.; Tiwari, P. M.; Eroglu, E.; Vig, K.; Dennis, V. A.; Singh, S. R. Functionalized Carbon Nanotubes: Biomedical Applications. *Int. J. Nanomed.* **2012**, *7*, 5361–5374.
22. Warheit, D. B.; Laurence, B. R.; Reed, K. L.; Roach, D. H.; Reynolds, G. A. M.; Webb, T. R. Comparative Pulmonary Toxicity Assessment of Single-Wall Carbon Nanotubes in Rats. *Toxicol. Sci.* **2004**, *77*, 117–125.

23. Lam, C. W.; James, J. T.; McCluskey, R.; Hunter, R. L. Pulmonary Toxicity of Single-Wall Carbon Nanotubes in Mice 7 and 90 Days after Intratracheal Instillation. *Toxicol. Sci.* **2004**, *77*, 126–134.
24. Wang, X.; Xia, T.; Ntim, S. A.; Ji, Z. X.; Lin, S. J.; Meng, H.; Chung, C. H.; George, S.; Zhang, H. Y.; Wang, M. Y.; *et al.* Dispersal State of Multiwalled Carbon Nanotubes Elicits Profibrogenic Cellular Responses That Correlate with Fibrogenesis Biomarkers and Fibrosis in the Murine Lung. *ACS Nano* **2011**, *5*, 9772–9787.
25. Wang, X.; Xia, T. A.; Duch, M. C.; Ji, Z. X.; Zhang, H. Y.; Li, R. B.; Sun, B. B.; Lin, S. J.; Meng, H.; Liao, Y. P.; *et al.* Pluronic F108 Coating Decreases the Lung Fibrosis Potential of Multiwall Carbon Nanotubes by Reducing Lysosomal Injury. *Nano Lett.* **2012**, *12*, 3050–3061.
26. Wang, X.; Zang, J. J.; Wang, H.; Nie, H.; Wang, T. C.; Deng, X. Y.; Gu, Y. Q.; Liu, Z. H.; Jia, G. Pulmonary Toxicity in Mice Exposed to Low and Medium Doses of Water-Soluble Multi-Walled Carbon Nanotubes. *J. Nanosci. Nanotechnol.* **2010**, *10*, 8516–8526.
27. Tabet, L.; Bussy, C.; Setyan, A.; Simon-Deckers, A.; Rossi, M. J.; Boczkowski, J.; Lanone, S. Coating Carbon Nanotubes with a Polystyrene-Based Polymer Protects against Pulmonary Toxicity. *Part. Fibre Toxicol.* **2011**, *8*, 13.
28. Roda, E.; Coccini, T.; Acerbi, D.; Barni, S.; Vaccarone, R.; Manzo, L. Comparative Pulmonary Toxicity Assessment of Pristine and Functionalized Multi-Walled Carbon Nanotubes Intratracheally Instilled in Rats: Morphohistochemical Evaluations. *Histol. Histopath.* **2011**, *26*, 357–367.
29. Xia, T.; Kovochich, M.; Liong, M.; Zink, J. I.; Nel, A. E. Cationic Polystyrene Nanosphere Toxicity Depends on Cell-Specific Endocytic and Mitochondrial Injury Pathways. *ACS Nano* **2008**, *2*, 85–96.
30. Gonzalez-Dominguez, J. M.; Gonzalez, M.; Anson-Casaos, A.; Diez-Pascual, A. M.; Gomez, M. A.; Martinez, M. T. Effect of Various Aminated Single-Walled Carbon Nanotubes on the Epoxy Cross-Linking Reactions. *J. Phys. Chem. C* **2011**, *115*, 7238–7248.
31. Xu, M. S.; Li, J.; Iwai, H.; Mei, Q. S.; Fujita, D.; Su, H. X.; Chen, H. Z.; Hanagata, N. Formation of Nano-Bio-Complex as Nanomaterials Dispersed in a Biological Solution for Understanding Nanobiological Interactions. *Sci. Rep.* **2012**, *2*, 406.
32. Derjaguin, B.; Landau, L. Theory of the Stability of Strongly Charged Lyophobic Sols and of the Adhesion of Strongly Charged-Particles in Solutions of Electrolytes. *Prog. Surf. Sci.* **1993**, *43*, 30–59.
33. Zhang, H. Y.; Xia, T.; Meng, H.; Xue, M.; George, S.; Ji, Z. X.; Wang, X.; Liu, R.; Wang, M. Y.; France, B.; *et al.* Differential Expression of Syndecan-1 Mediates Cationic Nanoparticle Toxicity in Undifferentiated *versus* Differentiated Normal Human Bronchial Epithelial Cells. *ACS Nano* **2011**, *5*, 2756–2769.
34. Okpalugo, T. I. T.; Papakonstantinou, P.; Murphy, H.; McLaughlin, J.; Brown, N. M. D. High Resolution XPS Characterization of Chemical Functionalised MWCNTs and SWCNTs. *Carbon* **2005**, *43*, 153–161.
35. Wang, X.; Xia, T. A.; Ntim, S. A.; Ji, Z. X.; George, S.; Meng, H. A.; Zhang, H. Y.; Castranova, V.; Mitra, S.; Nel, A. E. Quantitative Techniques for Assessing and Controlling the Dispersion and Biological Effects of Multiwalled Carbon Nanotubes in Mammalian Tissue Culture Cells. *ACS Nano* **2010**, *4*, 7241–7252.
36. Zhang, H. Y.; Ji, Z. X.; Xia, T.; Meng, H.; Low-Kam, C.; Liu, R.; Pokhrel, S.; Lin, S. J.; Wang, X.; Liao, Y. P.; *et al.* Use of Metal Oxide Nanoparticle Band Gap To Develop a Predictive Paradigm for Oxidative Stress and Acute Pulmonary Inflammation. *ACS Nano* **2012**, *6*, 4349–4368.
37. Malich, G.; Markovic, B.; Winder, C. The Sensitivity and Specificity of the MTS Tetrazolium Assay for Detecting the *In Vitro* Cytotoxicity of 20 Chemicals Using Human Cell Lines. *Toxicology* **1997**, *124*, 179–192.
38. Wilson, M. S.; Madala, S. K.; Ramalingam, T. R.; Gochuico, B. R.; Rosas, I. O.; Cheever, A. W.; Wynn, T. A. Bleomycin and Il-1 Beta-Mediated Pulmonary Fibrosis Is Il-17a Dependent. *J. Exp. Med.* **2010**, *207*, 535–552.
39. Bonner, J. C. Mesenchymal Cell Survival in Airway and Interstitial Pulmonary Fibrosis. *Fibrogenesis Tissue Repair* **2010**, *3*, 15.
40. Kayat, J.; Gajbhiye, V.; Tekade, R. K.; Jain, N. K. Pulmonary Toxicity of Carbon Nanotubes: A Systematic Report. *Nanomedicine* **2011**, *7*, 40–49.
41. Nagai, H.; Okazaki, Y.; Chew, S. H.; Misawa, N.; Yamashita, Y.; Akatsuka, S.; Ishihara, T.; Yamashita, K.; Yoshikawa, Y.; Yasui, H.; *et al.* Diameter and Rigidity of Multiwalled Carbon Nanotubes Are Critical Factors in Mesothelial Injury and Carcinogenesis. *Proc. Natl. Acad. Sci. U.S.A.* **2011**, *108*, E1330–E1338.
42. Castellano, F.; Montcourrier, P.; Chavrier, P. Membrane Recruitment of Rac1 Triggers Phagocytosis. *J. Cell Sci.* **2000**, *113*, 2955–2961.
43. Schroder, K.; Tschopp, J. The Inflammasomes. *Cell* **2010**, *140*, 821–832.
44. Dostert, C.; Petrilli, V.; Van Bruggen, R.; Steele, C.; Mossman, B. T.; Tschopp, J. Innate Immune Activation through Nalp3 Inflammasome Sensing of Asbestos and Silica. *Science* **2008**, *320*, 674–677.
45. Jin, C. C.; Flavell, R. A. Molecular Mechanism of Nlrp3 Inflammasome Activation. *J. Clin. Immunol.* **2010**, *30*, 628–631.
46. Hentze, H.; Lin, X. Y.; Choi, M. S. K.; Porter, A. G. Critical Role for Cathepsin B in Mediating Caspase-1-Dependent Interleukin-18 Maturation and Caspase-1-Independent Necrosis Triggered by the Microbial Toxin Nigericin. *Cell Death Differ.* **2003**, *10*, 956–968.
47. Porter, D. W.; Hubbs, A. F.; Mercer, R. R.; Wu, N.; Wolfarth, M. G.; Sriram, K.; Leonard, S.; Battelli, L.; Schwegler-Berry, D.; Friend, S.; *et al.* Mouse Pulmonary Dose- and Time Course-Responses Induced by Exposure to Multi-Walled Carbon Nanotubes. *Toxicology* **2010**, *269*, 136–147.
48. Shvedova, A. A.; Kisin, E. R.; Mercer, R.; Murray, A. R.; Johnson, V. J.; Potapovich, A. I.; Tyurina, Y. Y.; Gorelik, O.; Arepalli, S.; Schwegler-Berry, D.; *et al.* Unusual Inflammatory and Fibrogenic Pulmonary Responses to Single-Walled Carbon Nanotubes in Mice. *Am. J. Physiol.* **2005**, *289*, L698–L708.
49. Gasse, P.; Mary, C.; Guenon, I.; Noulin, N.; Charron, S.; Schnyder-Candrian, S.; Schnyder, B.; Akira, S.; Quesniaux, V. F. J.; Lagente, V.; *et al.* Il-1r1/Myd88 Signaling and the Inflammasome Are Essential in Pulmonary Inflammation and Fibrosis in Mice. *J. Clin. Invest.* **2007**, *117*, 3786–3799.
50. Kuzmych, O.; Allen, B. L.; Star, A. Carbon Nanotube Sensors for Exhaled Breath Components. *Nanotechnology* **2007**, *18*, 7.
51. Hu, X. G.; Wang, T.; Qu, X. H.; Dong, S. J. *In Situ* Synthesis and Characterization of Multiwalled Carbon Nanotube/Au Nanoparticle Composite Materials. *J. Phys. Chem. B* **2006**, *110*, 853–857.
52. Khaydarov, R. A.; Khaydarov, R. R.; Gapurova, O. Water Purification from Metal Ions Using Carbon Nanoparticle-Conjugated Polymer Nanocomposites. *Water Res.* **2010**, *44*, 1927–1933.
53. Hanzlikova, M.; Ruponen, M.; Galli, E.; Raasmaja, A.; Aseyev, V.; Tenhu, H.; Urtti, A.; Yliperttula, M. Mechanisms of Polyethylenimine-Mediated DNA Delivery: Free Carrier Helps To Overcome the Barrier of Cell-Surface Glycosaminoglycans. *J. Gene Med.* **2011**, *13*, 402–409.
54. Castranova, V.; Schulte, P. A.; Zumwalde, R. D. Occupational Nanosafety Considerations for Carbon Nanotubes and Carbon Nanofibers. *Acc. Chem. Res.* **2012**, 10.1021/ar300004a.
55. Kuempel, E. D.; Castranova, V.; Geraci, C. L.; Schulte, P. A. Development of Risk-Based Nanomaterial Groups for Occupational Exposure Control. *J. Nanopart. Res.* **2012**, 14.
56. Han, J. H.; Lee, E. J.; Lee, J. H.; So, K. P.; Lee, Y. H.; Bae, G. N.; Lee, S. B.; Ji, J. H.; Cho, M. H.; Yu, I. J. Monitoring Multiwalled Carbon Nanotube Exposure in Carbon Nanotube Research Facility. *Inhal. Toxicol.* **2008**, *20*, 741–749.
57. NIOSH Current Intelligence Bulletin: Occupational Exposure to Carbon Nanotubes and Nanofibers. 2010, www.cdc.gov/niosh/docket/review/docket161A/.

58. Porter, D. W.; Hubbs, A. F.; Mercer, R. R.; Wu, N. Q.; Wolfarth, M. G.; Sriram, K.; Leonard, S.; Battelli, L.; Schwegler-Berry, D.; Friend, S.; *et al.* Mouse Pulmonary Dose- and Time Course-Responses Induced by Exposure to Multi-Walled Carbon Nanotubes. *Toxicology* **2010**, *269*, 136–147.
59. Stone, K. C.; Mercer, R. R.; Gehr, P.; Stockstill, B.; Crapo, J. D. Allometric Relationships of Cell Numbers and Size in the Mammalian Lung. *Am. J. Respir. Cell Mol. Biol.* **1992**, *6*, 235–243.
60. Hinderliter, P. M.; Minard, K. R.; Orr, G.; Chrisler, W. B.; Thrall, B. D.; Pounds, J. G.; Teeguarden, J. G. Isdd: A Computational Model of Particle Sedimentation, Diffusion and Target Cell Dosimetry for *In Vitro* Toxicity Studies. *Part. Fibre Toxicol.* **2010**, *7*, 20.
61. Ji, Z.; Wang, X.; Zhang, H.; Lin, S.; Meng, H.; Sun, B.; George, S.; Xia, T.; Nel, A. E.; Zink, J. I. Designed Synthesis of CeO_2 Nanorods and Nanowires for Studying Toxicological Effects of High Aspect Ratio Nanomaterials. *ACS Nano* **2012**, *6*, 5366–5380.